JANUARY 23 2024

Acoustic metasurfaces with Frieze symmetries[a)]

D. B. Moore ; T. A. Starkey ; G. J. Chaplain

J. Acoust. Soc. Am. 155, 568–574 (2024)
https://doi.org/10.1121/10.0024359

JASA ARTICLE

Acoustic metasurfaces with Frieze symmetries[a]

D. B. Moore,[b] T. A. Starkey, and G. J. Chaplain
Centre for Metamaterial Research and Innovation, Department of Physics and Astronomy, University of Exeter, Exeter EX4 4QL, United Kingdom

ABSTRACT:
Frieze patterns follow a set of tiling instructions including reflection, rotation, and translation, and tile the infinite strip. Many metamaterials function due to the underlying symmetry, and its strategic breaking, of their constituent sub-structures that allow tailoring of the dispersion of modes supported by the structure. We design, simulate, and experimentally characterize seven one-dimensional acoustic metasurfaces whose unit cells each belong to one of the distinct Frieze groups.
https://doi.org/10.1121/10.0024359

(Received 10 October 2023; revised 30 November 2023; accepted 29 December 2023; published online 23 January 2024)
[Editor: Vladislav Sergeevich Sorokin] Pages: 568–574

I. INTRODUCTION

Utilizing the symmetry and translation of simple, or complex designs is as prevalent in decorating ancient pottery[1,2] as it has been over the last few decades in the engineering of dispersive metamaterials.[3,4] The effects of symmetry, and its strategic breaking, have been utilized across wave physics, from the passive beam-steering applications to topological surfaces and insulators.[5–10]

There has been a recent interest in the design of reconfigurable one-dimensional (1D) waveguiding structures,[11–14] whereby the symmetries of the unit cell are used, or broken, to tailor the dispersion of supported modes. Glide-symmetry has been extensively investigated in the electromagnetic regime,[15–18] with notable studies done by Hessel *et al*. in 1973[19] with periodically loaded waveguides. Glide-symmetry is a translation along a line followed by a reflection over that line; its uses in wave systems have recently been extended to acoustics[20–23] where the band-pinching effect has been utilized to create broadband regions of sub-sonic sound. A typical dispersion relation of a system with glide-symmetry has band-gaps that close, i.e., the bands "pinch," at the first Brillouin zone boundary (BZB), leading to locally linear dispersion, analogous to Dirac points and cones in electron bands.[24–27] Degeneracies at wavevectors not equal to the first BZB are referred to as accidental, i.e., the phenomena of "band-sticking" is where a pair of modes "stick" together due to the imposed degeneracy of the symmetry.[28–30]

Other possible unit cell symmetries are mirror translations (horizontal and vertical), that have been implemented in the design of tunable band-gaps in acoustic waveguides[31] as well as in conjunction with rotational symmetry in the case of topological insulators.[32–34] One particular set of motifs that utilize these operations (in addition to glide reflections) are Frieze patterns, whose elements, along with these operations, form a mathematical group. A Frieze group is then formally a class of infinite discrete symmetry groups of patterns on a strip.[35] The spectral properties of wave systems composed of structures with such symmetries have received recent attention,[36] with applications in nonreciprocal waveguiding in the presence of external fields.[37,38]

Despite the wealth of literature on the properties of glide-symmetric structures, across several wave domains,[17–19,21,39,40] and whilst the wave-dynamics of systems underpinned by Frieze geometries (and general space groups) is well established,[41–43] there is a lack of a comprehensive experimental review of the dispersive properties of acoustic waveguides that possess Frieze symmetries.

In this paper we seek to fill this gap and show how deliberate use of symmetry and translation conditions can be applied to an acoustic metasurface, ensuring that it belongs to one of the seven distinct Frieze groups. We experimentally and numerically (using finite elements) model the dispersion of its supported modes through the strategic breaking of these symmetries, and provide an overview of the dispersive properties of all seven Frieze groups that provides motivation towards their combinations for waveguiding applications. The metasurfaces are 3D printed and formed from arrays of rectangular cavities that couple through diffractive near-fields along the surface, and through submerged meander channels within the substrate. Altering the form of the meander, i.e., removing it entirely, and changing the boundary conditions of the cavities at the surface replicates structures that belong to each of the Frieze groups.

This paper is structured as follows: Section II briefly introduces Frieze groups, and a description of acoustic metamaterials. Section III brings these concepts together and

[a]This paper is part of a special issue on Wave Phenomena in Periodic, Near-Periodic, and Locally Resonant Systems.
[b]Email: dm680@exeter.ac.uk

describes acoustic waveguides obeying these Frieze symmetries. Section IV describes the methods. Section V presents the results and discussion.

II. BACKGROUND

A. Frieze groups

Frieze groups are two-dimensional line groups whose constituent patterns tile along a line to form a 1D periodic lattice: the infinite strip. There are seven unique Frieze groups which describe the invariance of a particular pattern, forming the unit cell, that tiles the strip under the operations of translation, horizontal, and vertical reflections, and rotations in the plane. Here, following similar notation to Ref. 37 we consider a unit cell that is a-periodic in the x direction, with the seven Frieze patterns defined in the x-y plane. The associated symmetry operators are translation, horizontal reflection, vertical reflection, and rotation, each defined, respectively, as

$$
\begin{aligned}
&\hat{T}_\alpha(x,y) \mapsto (x+\alpha, y),\\
&\hat{R}_h(x,y) \mapsto (x, -y),\\
&\hat{R}_v(x,y) \mapsto (-x, y),\\
&\hat{R}_\pi(x,y) \mapsto (-x, -y),
\end{aligned}
\tag{1}
$$

where $\alpha = a$ defines the 1D periodicity of the unit cell in x; all Frieze symmetry groups are invariant under $\hat{T}_a$. An important combination of two of these operations is a glide reflection that combines a horizontal translation and reflection about the axis of translation, namely, $\hat{R}\hat{T}_\alpha(x,y)$ such that $\alpha < a$. We will see the importance of defining several Frieze groups under a specific case of this which we define as $\hat{G}(x,y) \equiv \hat{R}\hat{T}_{a/2}(x,y)$; when referring to glide reflections we will explicitly assume the operation of $\hat{G}(x,y)$.

We introduce seven examples of the Frieze groups (F_n) in Fig. 1, following the notation from the International Union of Crystallography (IUC), used to identify members of wallpaper groups through four characters; the operations underpinning each symmetry group are encoded within a series of numbers and the letters. First, as each of the Frieze patterns form a primitive group the naming convention starts with the letter p, followed by a number that denotes the n-fold rotation of the pattern. The following two characters then describe two reflections with vertical mirrors first (horizontal reflection), and horizontal mirrors second (vertical reflection), both denoted by m, with glide reflections denoted g.[37,44,45] If there is either no rotational or mirror/glide symmetries present a place holder "1" denotes an orthogonal direction with no reflections. Applying IUC notation, we identify some examples: (i) The $p1$ symmetry has only translation symmetry $\hat{T}_\alpha$, i.e., is covered by one full rotation of 2π with all m, g omitted. (ii) $p1m1$ has a single vertical mirror symmetry $\hat{R}_v$. (iii) $p2mg$ contains a twofold rotational symmetry $\hat{R}_\pi$, a single vertical mirror plane and a glide translation. (iv) $p2mm$ contains a twofold rotational symmetry and both vertical and horizontal mirror reflections. There are, of course, other crystallographic notations such as Conway and Coxeter notation one could adopt.[46] In Fig. 1 we show schematics of "ball-and-stick" patterns that represent the seven Frieze groups. The ball-and-stick notation we present has a physical interpretation that represents the acoustic channels and boundary conditions that we detail below.

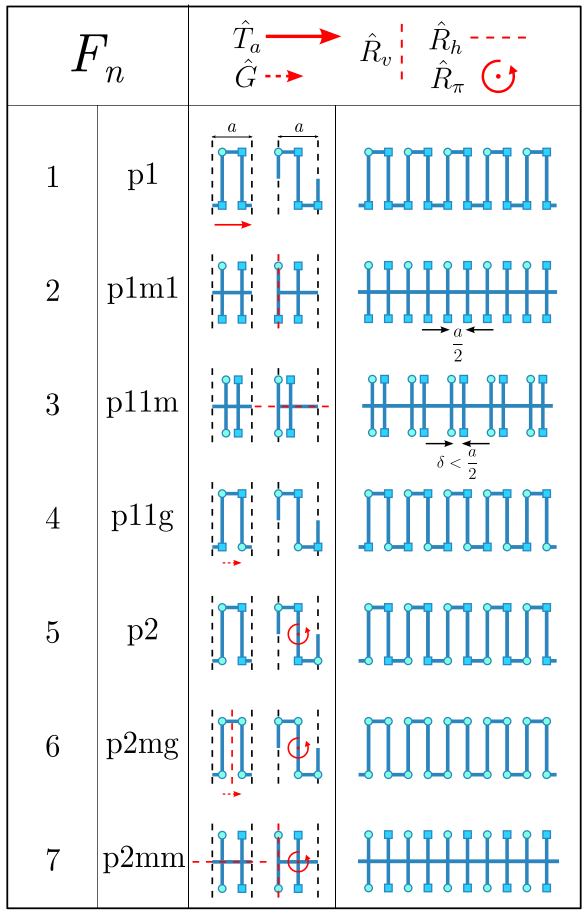

FIG. 1. (Color online) Table of the seven Frieze groups, F_n, with IUC notation. Symmetry operations are shown schematically in red. Two unit cells are shown for each group (dashed vertical black lines), along with five repeated cells showing the Frieze pattern. The "ball-and-stick" patterns correspond to the acoustic properties of the metasurface detailed in Fig. 2.

B. Acoustic waveguides with metamaterial concepts

Acoustic metasurfaces are commonly comprised of an array of periodically spaced resonators, separated by a distance λ_p, with the canonical example being cavities that couple to their nearest neighbors through the diffractive near-field.[47] We assume the substrate is acoustically rigid (sound hard). Under these conditions, an acoustic surface wave (ASW) can be formed, localized at the interface between the metasurface and the surrounding fluid, decaying evanescently from the surface,[22,31,47,48] analogous to electromagnetic spoof-surface plasmons on perfectly conducting patterned substrates.[49,50] In such a system, with a reciprocal lattice vector of size $|\boldsymbol{G}| = 2\pi/\lambda_p$, the dispersion curves contains a fundamental mode that approaches the first BZB with vanishing group velocity (and well defined asymptotic frequency[20]) whereby a standing wave is formed along the surface due to Bragg scattering.[51]

Crucially the cavity feature size is sub-wavelength with respect to the free-space acoustic wave at the same frequency. A similar asymptotic, slow-sound, character can been seen when the simple resonant cavity is replaced with a compact continuous meander channel, or space-coiled design.[20,52–55] In such a system, sound is forced to propagate through a channel which is longer than the external unit-cell length, leading to an increased effective refractive index.[20] The sound which travels through these channels accumulates a large phase delay compared to the free-space wave which, when mixed, can be used in the design of 1D waveguides with broadband frequency ranges of slow sound.

In Sec. III we describe a systematic approach to applying symmetry conditions to a particular pattern so to design acoustic metasurfaces, whose underlying unit cell belongs to a Frieze group.

III. FRIEZE-GROUP WAVEGUIDE DESIGN

Having introduced the key concepts and notation surrounding the Frieze groups, we now combine the two concepts in the design of a 1D waveguide with Frieze symmetries. To generate a physical system for experimental analysis, we take each of the patterns presented in Fig. 1 and we assign some physical properties. First, we identify the blue connecting lines form an acoustic channel, embedded in some 3D printed structure, in which sound can propagate. At junctions along this channel, we place two nodes, either turquoise circles or blue squares, that represent two boundary conditions with the former being an open boundary and the latter being a closed boundary. In the case of the metasurface design, these nodes occur at the surface of the structure, with the open boundaries permitting sound to travel along the surface of the waveguide via diffraction. The closed, or sound-hard, boundaries are achieved by covering the relevant openings at the surface. In practice this is done with a thick layer of adhesive tape so to not alter the path length of the cavities.

In Fig. 2 we show three configurations of the 3D printed unit cells, with example closed/open boundaries and their representative ball and stick diagrams. We note that the Frieze pattern is preserved in the cross section along the centre of the unit cell as our structures are obviously three dimensional, whilst the Frieze pattern itself is two dimensional. The acoustic channel is thus a void in the 3D printed structure of thickness t. We stress that with only these three unit cells, along with the relevant boundary conditions, we can recover all seven Frieze patterns. Figure 2(a) shows a unit cell with a meander structure that inherently breaks horizontal mirror symmetry and so covers the cases of $p1$, $p11g$, $p2$, and $p2mg$, whilst Fig. 2(b) contains no meander (a straight through channel) that allows $p1m1$ and $p2mm$ to be realized. For the particular case of $p11m$, we have only a horizontal mirror symmetry; we are therefore free to break

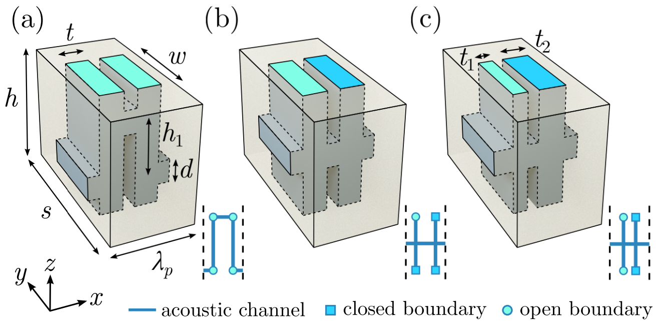

FIG. 2. (Color online) Example unit cell geometries: 3D printed PLA (cream colour) with acoustic channel (void) highlighted in blue-gray. Example open/closed boundaries are shown in turquoise and light blue, respectively, with representative ball-and-stick diagrams shown. Example Frieze groups are shown with (a) $p2mg$, (b) $p1m1$, and (c) $p11m$. The dimensions are detailed such that the cavities height $h = 30$ mm, thickness $t = 4$ mm, and width $w = 15$ mm. The unit-cell has a periodicity $\lambda_p = 12$ mm. Connecting channels have thickness $d = 4$ mm and are spaced symmetrically $h_1 = \pm 9.75$ mm about the centre of the cavity height. The cavity widths are revised in (c) for the $p11m$ pattern with $t_1 = 4$ mm and $t_2 = 2$ mm.

the vertical mirror symmetry by ensuring the separation of the channels (with different boundary conditions) is $<a/2$ (see Fig. 1). In practice, for the dimensions detailed in Fig. 2 and for the printing filament used (see below), this results in the wall separating the two channels becoming too thin, leading to coupling to the elastic motion of the wall. To avoid this and the undesirable result that the boundary can no longer be considered sound hard, we instead alter the thickness of the two channels such that $t_1 \neq t_2$ in Fig. 2(c). This is equivalent to breaking the vertical mirror symmetry shown by F_3 in Fig. 1.

We then form a 1D periodic array, comprising of 40 unit cells, for each of the configurations shown in Fig. 2. The result is three acoustic metasurfaces whose dispersion is dictated by the combination of the periodic cavity array and the waveguide-like meander/through-channels. For the cases of the through-channel, i.e., removing the meander, the substrate depth forms a singular channel through the length of the sample, resembling a loaded waveguide. In all cases, the structures support coupled waveguide modes; energy can propagate along the surface of the array and through the waveguide channels. The dispersive characteristics of each array are ultimately dictated by the underlying symmetry group of the unit cell, i.e., the length and form of the waveguide channels and the boundary conditions at the surface. In Sec. IV we detail the experimental and numerical methods used to verify the dispersive properties of the structure.

IV. METHODS

A. Sample fabrication

Samples are fabricated with a Ultimaker S5 3D printer. Polylactic acid (PLA) filament is printed with a 40% infill density to ensure acoustically rigid exterior and interior boundaries. The external dimensions of each sample are: thickness $h = 30$ mm, width $s = 35$ mm, and total length $L_{\text{total}} = 480$ mm comprised of 40 unit cells with periodicity

$\lambda_p = 12\,\text{mm}$. The internal dimensions for each unit cell are detailed in Fig. 2.

B. Acoustic measurements

Near-field acoustic measurements are performed by measuring the evolution of an acoustic pulse along the waveguide. Samples are excited by a tweeter (Scanspeak R3004/602000 26 mm) mounted within a conical attachment with a 3 mm exit diameter. The loudspeaker is driven by an arbitrary waveform generator (Keysight 33500B) producing single-cycle Sine-Gaussian pulses centred at $f_c = 8\,\text{kHz}$. The loudspeaker exit aperture is positioned over the first open cavity to excite the acoustic modes, see Fig. 3 for illustrative render.

The ASW pressure field is measured with a needle microphone (Brüel & Kjaer Probe Microphone type 4182) positioned 0.5 mm above the centre of the open cavities. Acoustic data are recorded by an oscilloscope (Picoscope 5000a) at sampling frequency $f_s = 312.5\,\text{kHz}$. The microphone is mounted on a motorized xy scanning stage (in-house with Aerotech controllers) and scanned with 0.45 mm step-size for length 474 mm in the propagation direction to spatially map the acoustic signal. An average was taken over eight measurements at each spatial position to improve the signal-to-noise ratio.

Acoustic data are analysed using Fourier techniques to obtain the wavenumber-frequency dependence of the localized waves. The fast-Fourier transform (FFT) (operator $\mathcal{F}$) of the measured signal, voltage $V(x, t)$ returns the complex Fourier amplitude in terms of the wavenumber parallel to the surface $k_\parallel$ and frequency f $\mathcal{F}_x(|\mathcal{F}_t(V(x,t))|)$. Data are windowed using a Tukey window, and zero-padded (in both space and time) by a factor of 2, before the FFT. These dispersion data are normalized by the maximum value at each frequency.

C. Numerical modeling

Numerical simulations are used to calculate the dispersion relations for each sample investigated. These were performed with finite element package COMSOL MULTIPHYSICS (version 6.0).[56] Using the pressure acoustics module, unit cell geometries were represented and assigned appropriate boundary conditions to approximate the physical system; Floquet-periodic boundaries were applied to represent an infinite sample, and sound-hard boundary conditions approximate the walls of the designed waveguides. Simulations return eigenmodes as a function of in-plane wavenumber.

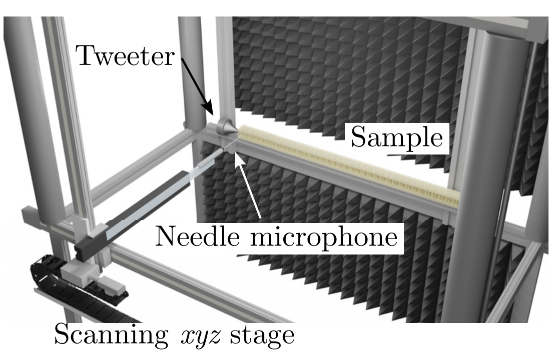

FIG. 3. (Color online) Render illustrating the acoustic measurement experiment; a loudspeaker mounted within a conical housing positioned at the end of the sample and the microphone positioned over the open cavities.

V. RESULTS

We fabricate, experimentally characterize, and numerically model the proposed acoustic waveguides obeying the Frieze symmetries (in Sec. III) using the methods described above. The results are collected and presented in Fig. 4. For each Frieze group we present the experimental characterization, with modelled eigenmodes, on the same dispersion plot within the first BZ. Due to our choice of spatial Fourier transform, positive and negative wavenumbers are equivalent; and modes that exist beyond the first BZ are band-folded to the first BZ, hence we show data from Γ to X only.

In all plots, the surface mode dispersion is presented below the sound-line (frequency $f = ck_0/2\pi$ with c the sound speed and k_0 the free space wavenumber), indicating the modes are sub-sonic and localized at the sample surface. The dark bands that disperse from the sound-line are the surface modes; we recall here that the X-point is the edge of the first Brillouin zone, i.e., $k_\parallel = \pi/\lambda_g$, and that the gradient these modes is the group velocity ($\boldsymbol{v}_g = \partial(\omega)/\partial\boldsymbol{k}$). In all cases the numerical model shows excellent agreement with experiment.

We present the discussion of these data in two parts: (1) for the meander-like samples with (a) $p2mg$, (b) $p11g$, (c) $p1$, and (d) $p2$ symmetries and then (2) for the loaded-waveguide samples with (e) $p2mm$, (f) $p11m$, and (g) $p1m1$ symmetries.

First, we consider the $p2mg$ and $p11g$ symmetries shown in Figs. 4(a), 4(b). The samples for these symmetries have the meander waveguide, with all cavities open ($p2mg$) at the surfaces above and below, or every other cavity open ($p11g$) as viewed by the wave in the waveguide.

In both cases, at low frequency a mode disperses from zero frequency/zero wavenumber up the sound-line, before dispersing with a near-constant gradient towards the first BZB at X. This band continues through the first BZ and is visualized in these diagrams as a "bandfolded" mode now dispersing back from the X-point toward Γ without any discontinuity in its Fourier amplitude. This demonstrates eigenmodes of the system that are degenerate at the first BZB.

Above the fundamental mode, a mode cuts on at higher frequency, dispersing up the sound-line before exhibiting the same dispersion from the sound-line. The region of linear dispersion exhibited as both modes leave the sound-line, is an expected consequence of the glide symmetry of the unit cell due to the meander structure.[20]

The difference between the frequency of each mode is due to the effective path length of the acoustic field within

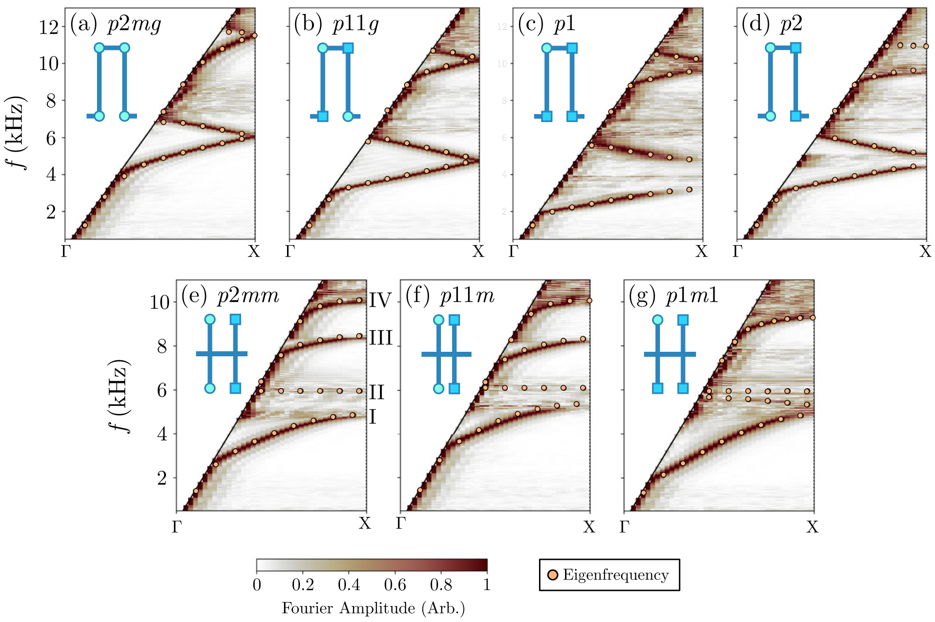

FIG. 4. (Color online) Experimental dispersion relations for Frieze group acoustic waveguides: (a) *p2mg*, (b) *p11g*, (c) *p1*, (d) *p2*, (e) *p2mm*, (f) *p11m*, and (g) *p1m1*. Insets show the pictorial representation of each Frieze group. Color maps represent the absolute value of the normalized Fourier spectra. Orange points are the eigensolutions from FEM simulations. Results are shown within the first Brillouin zone from the Γ-point ($k_{\|} = 0$) to the *X*-point ($k_{\|} = \pi/\lambda_g$).

the waveguide; the *p2mg* sample has all cavities open and disperses at relatively higher frequencies, when the cavities are closed the internal tortuous waveguide path is now longer, which pulls the frequencies of the guided acoustic waves to a lower frequency.

Next, we consider the *p1* and *p2* symmetries shown in Figs. 4(c), 4(d). Again, these are based on the meander waveguide, with selected cavities closed. The *p1* sample has three covered cavities, and *p2* has one cavity covered top and bottom. The key change between previous dispersion diagrams is that band-gaps have now opened at the *X*-point for both symmetries, i.e., the placement of these coverings has lifted the degeneracies seen in the previous two symmetry groups; this is expected for geometries than do not possess a glide symmetry. In these dispersion diagrams, the modes now meet the first Brillouin zone boundary ($|k_{\|}|$) with zero-gradient and, consequently, diminished Fourier amplitude, indicating reduced propagation down the sample length. The *p1* experimental data shows the modes exist at a reduced frequency due to the increased path length through the meander between open cavities. A band-split pair of the fundamental mode is shown in the first Brillouin zone in both symmetry cases, with the width of the gap influenced by the meander path length.

The higher-order modes, at approximately 10 kHz, are different between samples: in the *p1* sample data both band-split modes are detected, whilst for *p2*, the higher frequency mode is not detected at approximately 11 kHz as the model predicts. This is because the mode has a near-zero group velocity, and therefore cannot propagate from source to detector.

Finally, we compare the *p2mm*, *p11m*, and *p1m1* symmetries shown in Figs. 4(e)–4(g), respectively, where there is no meander present. These waveguides are an arrangement of adjacent cavities about a through cavity running the length of the sample. The cavities are either open or closed on the top and/or bottom of the waveguide to generate the symmetries of the groups. These arrangements allow coupled $\lambda/2$- or $\lambda/4$-like resonances of the cavities, and result in symmetric/anti-symmetric resonances depending on the positions of the open/closed boundary conditions.

Figures 4(e)–4(g) show the experimental results with the model eigenmodes overlaid. For these samples, the numerical model predicts four modes in the frequency range studied. The modes that disperse up and from the sound line are well resolved in all cases. The flat-banded modes are not resolved experimentally; this is due to distribution of the pressure field along the sample and is discussed and elucidated via a tabular notation which we which we highlight in Fig. 5. We adopt this notation for brevity in describing the many features of the dispersion relations. It is motivated by inspecting the eigenmodes obtained from numerical modelling, at the edge of the first BZ, which show the symmetries of the eigenmodes (dictated by the underlying Frieze patterns.).

Following the notation introduced in Fig. 5, the *p2mm* and *p11m* samples have the cavities are represented as open (o) and closed (c), arranged around the central waveguide (−). For *p2mm* the distribution is $\frac{\text{o} \quad \text{c}}{\text{o} \quad \text{c}}$.

The four modes predicted, in increasing frequency, have these allowed pressure field distributions at the cavity ends (following the tabular notation), at the BZB: $\frac{0 \quad +}{0 \quad +}$, $\frac{0 \quad +}{0 \quad -}$, $\frac{+ \quad 0}{+ \quad 0}$, and $\frac{+ \quad 0}{- \quad 0}$ (highlighted in Fig. 5). The first two pressure field distributions are the symmetric and anti-symmetric modes with fields concentrated in the close-ended cavities. The other two distributions are the symmetric/anti-symmetric mode-pair for fields in the open-ended cavities. The resonant frequencies are dictated by the effective volume of air within these structures.

The experimental data for *p2mm* and *p11m* is visually similar; three dispersing modes are measured. For the lowest

https://doi.org/10.1121/10.0024359

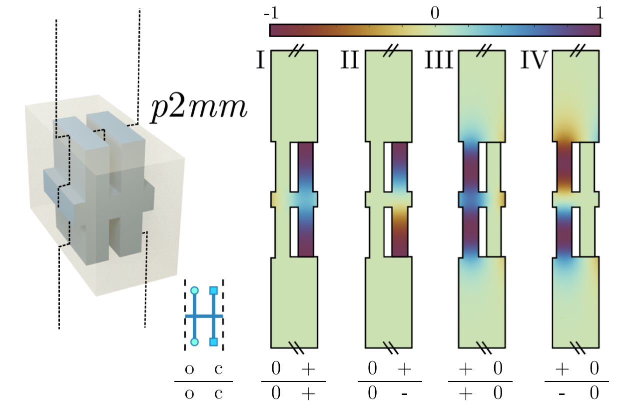

FIG. 5. (Color online) Eigenmodes and tabular notation of *p*2*mm* Frieze pattern: A schematic of the unit cell is shown with the dashed lines highlighting the plane at which the eigensolution is extracted from the numerical model. Shown too are the eigenmodes (color showing normalised pressure) at the BZB for the curves marked I–IV in Fig. 4(e). Floquet-Bloch boundary conditions are applied at the left and right sides, with radiation conditions top and bottom. Below we show two tabular notations: the first represents the cavity boundary conditions with open (o) and closed (c) representing the circles and squares of the ball-and-stick diagrams. Second, the symmetry of the mode-shapes are emphasised through the symbols +,−,0, representing maximum, minimum, and vanishing pressure, respectively, at the cavity opening/closings.

mode, $\dfrac{0 \quad +}{0 \quad +}$, the Fourier amplitude diminishes as the mode approaches the *X*-point, because the pressure field becomes localized in the closed-portion of the waveguide and presents a low amplitude (and decaying) pressure field at the open cavities. In contrast, the modes localized in the open cavities are detected experimentally through probing the pressure field at the surface.

In both cases, the mode predicted to meet the BZB at approximately 6 kHz, which corresponds to the $\dfrac{0 \quad +}{0 \quad -}$ pressure distribution, is not measured. This mode is flat-banded and highly localized in the waveguide because the field amplitude is zero between the closed-ended cavities due to the π-phase difference in pressure relative to one another. This prevents the mode from propagating through the structure.[13]

The final sample, *p*1*m*1, has 1 open and 3 closed cavities configured as $\dfrac{\mathrm{o} \quad \mathrm{c}}{\mathrm{c} \quad \mathrm{c}}$. The results [Fig. 4(g)] show two clearly resolved modes approaching the BZB at approximately 5 and 9.5 kHz, and two flat bands predicted by the numerical model, but not experimentally observed. Here, by replacing on open cavity with a closed cavity the $\dfrac{+ \quad 0}{+ \quad 0}$, mode has become flat-banded and reduced in frequency as the closed boundary condition has reduced the effective cavity volume.

VI. CONCLUSIONS

We have manufactured three samples, patterned with a 1D array of resonant cavities while concealing additional connective channels within the substrate. Through strategic replacement of open boundary conditions with sound-hard, these three unit cells can inherit the symmetry properties of all seven Frieze groups. The dispersion of the supported modes changes whether or not the structure obtains a glide reflection, where band-pinching is observed at the edge of the first BZB, resulting in locally linear dispersion and slow sound. Whilst we chose to implement the various Frieze symmetries via modification to open or closed boundary conditions, we note that it is possible to obtain the same effects through modification (by shape or size) to the unit-cell structure factor. The presented results form a comprehensive experimental summary of acoustic metasurfaces possessing Frieze symmetries that provides motivations for their combinations which finds uses in designing acoustic devices for sensing applications using regions of sub-sonic sound to increase sensitivity within a fixed frequency range and engineering interface states for 1D topological surfaces[23] using common band-gaps between different symmetries.

ACKNOWLEDGMENTS

The authors wish to acknowledge financial support from the Engineering and Physical Sciences Research Council (EPSRC) of the United Kingdom via the EPSRC Centre for Doctoral Training in Metamaterials (Grant No. EP/ L015331/ 1). D.B.M. and T.A.S. acknowledge the financial support of Defence Science and Technology Laboratory (DSTL) through Grants Nos. DSTLXR1000154754 and AGR 0117701. G.J.C. gratefully acknowledges financial support from the Royal Commission for the Exhibition of 1851 in the form of a Research Fellowship. The authors are grateful to Professor A. P. Hibbins and Professor Sir J. R. Sambles for useful conversations.

AUTHOR DECLARATIONS

Conflict of Interest

The authors declare no competing interests.

DATA AVAILABILITY

All data created during this research are openly available from the University of Exeter institutional repository.[57]

[1]E. Makovicky, *Symmetry: Through the Eyes of Old Masters*, 1st ed. (Walter de Gruyter, New York, 2016).
[2]U. Bismayer, S. Srilomsak, Y. Treekamol, W. Tanthanuch, and K. Suriyatham, "Artefacts from Ban Chiang, Thailand: Pottery with hematite-red geometric patterns," Z. Kristallogr. – Cryst. Mater. **235**(11), 559–568 (2020).
[3]N. Engheta and R. W. Ziolkowski *Metamaterials: Physics and Engineering Explorations* (Wiley-IEEE, New York, 2006).
[4]G. Ma and P. Sheng, "Acoustic metamaterials: From local resonances to broad horizons," Sci. Adv. **2**(2), e1501595 (2016).
[5]H.-S. Lai, Y.-L. Xu, B. He, X.-C. Sun, C. He, and Y.-F. Chen, "Tunable topological surface states of three-dimensional acoustic crystals," Front. Phys. **9**, 789697 (2021).
[6]Z.-K. Lin, Y. Wu, B. Jiang, Y. Liu, S.-Q. Wu, and F. Li, "Topological Wannier cycles induced by sub-unit-cell artificial gauge flux in a sonic crystal Zhi-Kang," Nat. Mater. **21**(4), 430–437 (2022).

[7]N. Laforge, V. Laude, F. Chollet, A. Khelif, M. Kadic, Y. Guo, and R. Fleury, "Observation of topological gravity-capillary waves in a water wave crystal," New J. Phys. **21**(8), 083031 (2019).
[8]A. Darabi and M. J. Leamy, "Reconfigurable topological insulator for elastic waves," J. Acoust. Soc. Am. **146**(1), 773–781 (2019).
[9]H. Fan, B. Xia, L. Tong, S. Zheng, and D. Yu, "Elastic higher-order topological insulator with topologically protected corner states," Phys. Rev. Lett. **122**(20), 204301 (2019).
[10]Y. Chen, D. Liu, Y. Wu, P. Yu, and Y. Liu, "Valley Hall elastic topological insulator with large Chern numbers," Int. J. Mech. Sci. **239**, 107884 (2023).
[11]S. Periyannan, P. Rajagopal, and K. Balasubramaniam, "Re-configurable multi-level temperature sensing by ultrasonic 'spring-like' helical waveguide," J. Appl. Phys. **119**(14), 144502 (2016).
[12]M. J. Frazier, "Multi-stable acoustic metamaterials with re-configurable mass distribution," J. Appl. Phys. **131**(16), 165105 (2022).
[13]D. B. Moore, G. P. Ward, J. D. Smith, A. P. Hibbins, J. R. Sambles, and T. A. Starkey, "Confined acoustic line modes within a glide–symmetric waveguide," Sci. Rep. **12**(1), 10954 (2022).
[14]G. J. Chaplain, I. R. Hooper, A. P. Hibbins, and T. A. Starkey, "Reconfigurable elastic metamaterials: Engineering dispersion with beyond nearest neighbors," Phys. Rev. Appl. **19**(4), 044061 (2023).
[15]F. Maurin, C. Claeys, L. Van Belle, and W. Desmet, "Bloch theorem with revised boundary conditions applied to glide, screw and rotational symmetric structures," Comput. Methods Appl. Mech. Eng. **318**, 497–513 (2017).
[16]B. Fischer and G. Valerio, "Wideband homogenization of a glide-symmetric holey parallel-plate waveguide," in *Ursi Gass 2021*, Rome, Italy (2021), Vol. 1.
[17]O. Quevedo-Teruel, C. Qiao, F. Mesa, N. Fonseca, and G. Valerio, "On the benefits of glide symmetries for microwave devices," IEEE J. Microwave **1**(1), 457–469 (2021).
[18]P. Zhang, "Symmetry and degeneracy of phonon modes for periodic structures with glide symmetry," J. Mech. Phys. Solids **122**, 244–261 (2019).
[19]A. Hessel, M. H. U. I. Chen, C. M. Robert, and A. A. Oliner, "Propagation in periodically loaded waveguides with higher symmetries," Proc. IEEE **61**(2), 183 (1973).
[20]J. G. Beadle, I. R. Hooper, J. R. Sambles, and A. P. Hibbins, "Broadband, slow sound on a glide-symmetric meander-channel surface," J. Acoust. Soc. Am. **145**(5), 3190–3194 (2019).
[21]N. Janković and A. Alù, "Glide-symmetric acoustic waveguides for extreme sensing and isolation," Phys. Rev. Appl. **15**(2), 024004 (2021).
[22]G. P. Ward, J. D. Smith, A. P. Hibbins, J. R. Sambles, and T. A. Starkey, "Gapless dispersion of acoustic line modes with glide symmetry," Phys. Rev. B **105**(24), 245401 (2022).
[23]J. A. I. Martínez, N. Laforge, M. Kadic, and V. Laude, "Topological waves guided by a glide-reflection symmetric crystal interface," Phys. Rev. B **106**(6), 064304 (2022).
[24]D. Torrent and J. Sánchez-Dehesa, "Acoustic analogue of graphene: Observation of Dirac cones in acoustic surface waves," Phys. Rev. Lett. **108**(17), 174301 (2012).
[25]S. Yves, F. Lemoult, M. Fink, and G. Lerosey, "Crystalline soda can metamaterial exhibiting graphene-like dispersion at subwavelength scale," Sci. Rep. **7**(1), 15359 (2017).
[26]T. A. Starkey, V. Kyrimi, G. P. Ward, J. R. Sambles, and A. P. Hibbins, "Experimental characterisation of the bound acoustic surface modes supported by honeycomb and hexagonal hole arrays," Sci. Rep. **9**(1), 15773 (2019).
[27]Z. Tian, C. Shen, J. Li, E. Reit, H. Bachman, J. E. Socolar, S. A. Cummer, and T. Jun Huang, "Dispersion tuning and route reconfiguration of acoustic waves in valley topological phononic crystals," Nat. Commun. **11**(1), 762 (2020).
[28]Y. H. J. Yau, P. I. Galich, and E. L. Thomas, "Designer band gaps in phononic crystals via nonsymmorphic symmetry," in *Proceedings of the 26th International Congress on Sound and Vibration, ICSV 2019* (2018), pp. 1–8.
[29]Y. Quan, V. Taufour, and W. E. Pickett, "Nonsymmorphic band sticking in a topological superconductor," Phys. Rev. B **105**(6), 064517 (2022).
[30]J. R. Badger, Y. Quan, M. C. Staab, S. Sumita, A. Rossi, K. P. Devlin, K. Neubauer, D. S. Shulman, J. C. Fettinger, P. Klavins, S. M. Kauzlarich, D. Aoki, I. M. Vishik, W. E. Pickett, and V. Taufour, "Dirac lines and loop at the Fermi level in the time-reversal symmetry breaking superconductor $LaNiGa_2$," Commun. Phys. **5**(1), 22 (2022).
[31]N. Cselyuszka, A. Alù, and N. Janković, "Spoof-fluid-spoof acoustic waveguide and its applications for sound manipulation," Phys. Rev. Appl. **12**(5), 054014 (2019).
[32]M. P. Makwana and R. V. Craster, "Geometrically navigating topological plate modes around gentle and sharp bends," Phys. Rev. B **98**(18), 184105 (2018).
[33]M. P. Makwana and G. Chaplain, "Tunable three-way topological energy-splitter," Sci. Rep. **9**(1), 18939 (2019).
[34]N. Laforge, R. Wiltshaw, R. V. Craster, V. Laude, J. A. I. Martínez, G. Dupont, S. Guenneau, M. Kadic, and M. P. Makwana, "Acoustic topological circuitry in square and rectangular phononic crystals," Phys. Rev. Appl. **15**(5), 054056 (2021).
[35]H. S. M. Coxeter, *Introduction to Geometry* (Wiley, New York, 1969).
[36]F. R. Lux, T. Stoiber, S. Wang, G. Huang, and E. Prodan, "Topological spectral bands with frieze groups," arXiv:2209.12306 (2022).
[37]Y. Mazor, Y. Hadad, and B. Z. Steinberg, "Planar one-way guiding in periodic particle arrays with asymmetric unit cell and general group-symmetry considerations," Phys. Rev. B **92**(12), 125129 (2015).
[38]O. Silbiger and Y. Hadad, "One-way acoustic guiding under transverse fluid flow," Phys. Rev. Appl. **17**(6), 064058 (2022).
[39]M. Camacho, R. C. Mitchell-Thomas, A. P. Hibbins, J. R. Sambles, and O. Quevedo-Teruel, "Mimicking glide symmetry dispersion with coupled slot metasurfaces," Appl. Phys. Lett **111**(12), 121603 (2017).
[40]M. Ebrahimpouri, O. Quevedo-Teruel, and E. Rajo-Iglesias, "Design guidelines for gap waveguide technology based on glide-symmetric holey structures," IEEE Microwave Wireless Compon. Lett. **27**(6), 542–544 (2017).
[41]A. König and N. D. Mermin, "Electronic level degeneracy in nonsymmorphic periodic or aperiodic crystals," Phys. Rev. B **56**(21), 13607 (1997).
[42]A. Mock, L. Lu, and J. O'Brien, "Space group theory and Fourier space analysis of two-dimensional photonic crystal waveguides," Phys. Rev. B **81**(15), 155115 (2010).
[43]M. S. Dresselhaus, G. Dresselhaus, and A. Jorio, *Group Theory: Application to the Physics of Condensed Matter* (Springer Science & Business Media, New York, 2007).
[44]Y. Liu, R. T. Collins, and Y. Tsin, "A computational model for periodic pattern perception based on frieze and wallpaper groups," IEEE Trans. Pattern Anal. Mach. Intell. **26**(3), 354–371 (2004).
[45]A. Katsap and F. L. Silverman, "Transformations, shapes and patterns analysis in the Negev Bedouins' embroideries," in *Ethnomathematics of Negev Bedouins' Existence in Forms, Symbols and Geometric Patterns* (Brill, Leiden, 2016), pp. 69–166.
[46]J. H. Conway, H. Burgiel, and C. Goodman-Strauss, *The Symmetries of Things* (CRC Press, Boca Raton, FL, 2016).
[47]L. Kelders, J. F. Allard, and W. Lauriks, "Ultrasonic surface waves above rectangular-groove gratings," J. Acoust. Soc. Am. **103**(5), 2730–2733 (1998).
[48]J. A. Iglesias Martínez, M. F. Groß, Y. Chen, T. Frenzel, V. Laude, M. Kadic, and M. Wegener, "Experimental observation of roton-like dispersion relations in metamaterials," Sci. Adv. **7**(49), eabm2189 (2021).
[49]J. Pendry, L. Martin-Moreno, and F. Garcia-Vidal, "Mimicking surface plasmons with structured surfaces," Science **305**(5685), 847–848 (2004).
[50]N. Janković, S. Ilić, V. Bengin, S. Birgermajer, V. Radonić, and A. Alu, "Acoustic spoof surface plasmon polaritons for filtering, isolation and sensing," Res. Phys. **28**, 104645 (2021).
[51]G. P. Ward, A. P. Hibbins, J. R. Sambles, and J. D. Smith, "The waveguiding of sound using lines of resonant holes," Sci. Rep. **9**(1), 7–11 (2019).
[52]Z. Liang and J. Li, "Extreme acoustic metamaterial by coiling up space," Phys. Rev. Lett. **108**, 114301 (2012).
[53]M. Yang, S. Chen, C. Fu, and P. Sheng, "Optimal sound-absorbing structures," Mater. Horiz. **4**(4), 673–680 (2017).
[54]S. Degraeve and J. Oclee-Brown, "Metamaterial absorber for loudspeaker enclosures," Audio Eng. Soc. Conv. **148**, 10341 (2020).
[55]S. R. Shelley, J. G. Beadle, A. P. Hibbins, and J. R. Sambles, "Slow acoustic surface modes through the use of hidden geometry," Sci. Rep. **11**(1), 22010 (2021).
[56]COMSOL Multiphysics, v. 6.0, COMSOL AB, Stockholm, Sweden, www.comsol.com/ (Last viewed January 14, 2022).
[57]University of Exeter, https://ore.exeter.ac.uk/ (2024).